Analysis and optimization approach for the doped amorphous layers of silicon heterojunction solar cells

Damian Pysch,[1,a)] Christoph Meinhard,[1] Nils-Peter Harder,[2] Martin Hermle,[1] and Stefan W. Glunz[1]
[1]*Fraunhofer Institute for Solar Energy Systems, Heidenhofstr. 2, D-79110 Freiburg, Germany*
[2]*Institute for Solar Energy Research Hamelin (ISFH), Am Ohrberg 1, D-31860 Emmerthal, Germany*

(Received 23 May 2011; accepted 1 September 2011; published online 10 November 2011)

Comparison of the open-circuit voltage (external voltage $V_{oc,ext}$) determined by *Suns*-V_{oc} measurements with the implied voltage $V_{oc,impl}$ determined by transient photoconductance decay lifetime measurements can yield a quick and easy analysis of silicon heterojunction (SHJ) solar cells, especially in regard to finding the optimum doping concentration of the emitter layer [or back surface field (BSF)]. A sufficiently high doping concentration of the emitter and BSF is mandatory to extract the internal Fermi-level splitting and thus the internal voltage, at the solar cell contacts. However increasing the concentration of doping gases during the deposition of doped amorphous silicon layers results in a reduction of the interface passivation quality and $V_{oc,impl}$. The best trade off is realized when the ratio of $V_{oc,ext}$ to $V_{oc,impl}$ (external/internal V_{oc}-ratio ζ) reaches a saturation value near 1 upon increasing the doping concentration. AFORS-HET (Automat FOR Simulation of HETerostructures) simulations resulted in the conclusion that the characteristics of the external/internal V_{oc}-ratio are mainly determined by the active doping concentration (doping minus defect concentration). © *2011 American Institute of Physics*. [doi:10.1063/1.3650255]

I. INTRODUCTION

Silicon heterojunction (SHJ) solar cells are known to have the potential to produce open-circuit voltages above 700 mV.[1,2] In order to obtain such high voltages we need to guarantee a good passivation of the interface between the amorphous and the crystalline silicon (c-Si(n or p)), as well as an optimal doping of the emitter layer a-Si:H(p or n).[3] Currently the best performing SHJ solar cell approach is the heterojunction with an intrinsic thin layer (HIT) concept,[1] where a hydrogenated, intrinsic amorphous a-Si:H(i) layer passivates the interface while the doped amorphous silicon layers (a-Si:H(p or n)) form the actual emitter and the BSF.

Up to now, only few investigations were published in regard to an optimization of the doping concentration of the emitter or BSF of SHJ solar cell devices. Recently published results made use of advanced characterization methods[3–5] on simple, one-sided SHJ structures. Another approach is to process SHJ solar cell devices (including a metallization), vary the doping concentration of the doped layer, and monitor the V_{oc} of the finished solar cells.[4,6]

The challenge in the development of SHJ solar cells is to optimize both the interface passivation and the doping of the emitter/BSF at the same time. It is known from the advanced characterization methods like near-UV photoemission spectroscopy and surface photo voltage measurements that an excessively high doping of the a-Si:H(n) layer can lead to a reduction of the open-circuit voltage, due to an increasing defect concentration in the a-Si:H(n) layer.[3–5] An easy and fast-to-apply approach to monitor the influence of a variation of the doping concentration of the emitter/BSF layer is to compare the calculated, lifetime-based implied voltage $V_{oc,impl}$ with the actually measured external voltage $V_{oc,ext}$ (*Suns*-V_{oc} voltage at one sun).[7,8] $V_{oc,impl}$, i.e., the splitting of the quasi-Fermi levels represents the interface passivation quality and bulk recombination, whereas $V_{oc,ext}$ is additionally influenced by the active doping concentration of the emitter or BSF (discussed in more detail in Sec. III).

These measurements can be performed quickly and with simple setups. A comparison of the $V_{oc,impl}$ to $V_{oc,ext}$ can make the physical understanding and the process optimization of SHJ solar cells fast and effective.

II. EXPERIMENTAL

Charge carrier lifetime measurements by means of transient photoconductance decay and *Suns*-V_{oc} measurements were performed with a *Suns*-V_{oc} and QSSPC measurement setup by Sinton Instruments.[7,9,10]

The thickness of the a-Si:H layers was determined by spectroscopic ellipsometry. All measurements were performed using a J.A. Woollam C. VASE rotating analyzer ellipsometer. The angle of incidence was 70° and a Tauc-Lorentz-model was used to fit the data.[11] The error of the thickness measurement was determined by comparison of spectral ellipsometry and transmission electron microscopy measurements to around 0.5 nm.[11]

All a-Si:H(i,n,p), and indium tin oxide (ITO) layers were deposited using a "System 100 Pro", a multi PECVD chamber cluster tool by Oxford Instruments.

For this investigation full heterojunction V_{oc}-samples have been processed (see Fig. 1) on flat, n-type, crystalline silicon (c-Si(n)) wafers (FZ, 1 Ω cm, thickness = 210 μm). All wafers were wet-chemically oxidized in HNO_3. The

a)Author to whom correspondence should be addressed. Electronic mail: damian.pysch@ise.fraunhofer.de. FAX: +49-7614588250.

 © 2011 American Institute of Physics

Author complimentary copy. Redistribution subject to AIP license or copyright, see http://jap.aip.org/jap/copyright.jsp

grown chemical oxide was then removed by a short 1%-HF dip prior to the deposition of a thin, intrinsic, hydrogenated amorphous silicon layer (a-Si:H(i)).[12] The BSF on the rear side of all V_{oc}-samples was built of 5 nm a-Si:H(i), 15 nm n-doped, hydrogenated, amorphous silicon carbide a-SiC:H(n), and 80 nm ITO. On the front side also a 5 nm a-Si:H(i) layer was deposited. For the doped emitter layer (10 nm a-Si:H(p)), the doping gas concentration of diborane [B_2H_6] has been varied from 0 to 30 sccm.

For the optimization of the [B_2H_6] gas phase concentration during the deposition of the a-Si:H(p) layer we substituted the H_2 gas flow, which was already present for the optimized a-Si:H(i) deposition process[13] subsequently with the doping gas [B_2H_6] diluted in H_2 (concentration of 1% [B_2H_6] in H_2). Thus the total gas flow and ratio of H_2:SiH_4 remained approximately constant, with only the concentration of [B_2H_6] being varied.

III. EXPERIMENTAL RESULTS ON DOPING DEPENDENCE OF $V_{oc,ext}$ AND $V_{oc,impl}$

For SHJ solar cells including an ITO layer on the front and back side it is not necessary to process the metal contacts at the front and back side in order to analyze the influence of the doping concentration dependence of the emitter or BSF layer on the external voltage. It is possible to measure the $V_{oc,ext}$ value and the shape of the resulting series resistance-free *IV*-characteristic represented by the pseudo fill factor (PFF),[10,14] by application of the Sinton Instruments *Suns*-V_{oc} setup. If we further conduct a lifetime measurement using the Sinton Instruments WTC120 lifetime tester (in transient mode), the electron and hole carrier densities at an illumination density equal to one sun can be determined. This enables us to calculate the so-called implied voltage

$$V_{oc,impl} = \frac{k_B T}{q} \ln\left(\frac{pn}{n_i^2}\right). \quad (1)$$

T represents the temperature, k_B is the Boltzmann constant, q is the elementary charge, n is the electron concentration of the n-type wafer (which equals to the doping concentration in low level injection and to the excess carrier concentration for high level injection), p is the minority carrier (hole) density, and n_i is the intrinsic carrier density of crystalline silicon ($n_i = 10^{10}\,\mathrm{cm}^{-3}$). The implied voltage $V_{oc,impl}$ represents a measure of the interface passivation and bulk recombination and thus of the splitting of the quasi Fermi level within the wafer. This argument is based on the fact that a wafer passivated with just an intrinsic amorphous silicon layer can show a very high implied voltage; however, no external voltage can be determined (see Fig. 2, lowest [B_2H_6] concentrations). The $V_{oc,ext}$ value represents also a measure of interface passivation. However, additionally $V_{oc,ext}$ is influenced by internal voltage losses like gradients in the majority carrier quasi-Fermi level. For example, $V_{oc,ext}$ is influenced by the doping concentration built into the a-Si:H-layer. More precisely, $V_{oc,ext}$ is influenced by the ratio between the excess carrier density and the active doping concentration in the doped a-Si:H layer (see Sec. IV A and Eq. (5)). If the majority carrier concentration greatly exceeds the excess carrier concentration at the contacted regions the actually measurable voltage $V_{oc,ext}$ represents the energy difference between the electron and hole Fermi levels at the n-type and p-type contact, respectively. Thus $V_{oc,impl}$ is always the upper limit of $V_{oc,ext}$.

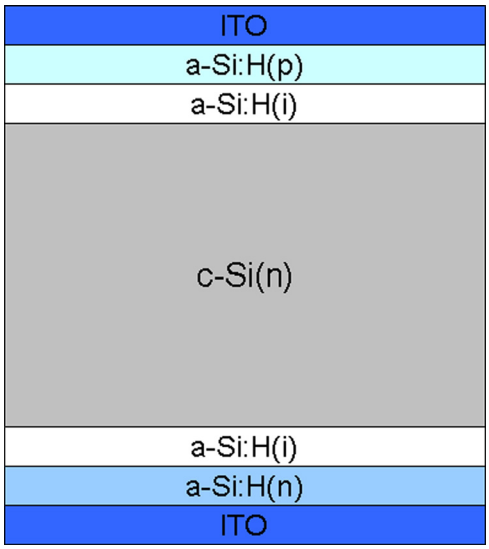

FIG. 1. (Color online) Structure of SHJ V_{oc}-sample on an n-type c-Si wafer. Such V_{oc}-samples were used for all investigations in this publication.

The rear sides of the V_{oc}-samples shown in Fig. 1 consist of a layer stack as described in the Experimental section and is assumed to create an ideal BSF, which is not limiting the performance of the sample. The dependence of $V_{oc,ext}$ and the $V_{oc,impl}$ on an increasing [B_2H_6] concentration is shown in Fig. 2. An increase of the doping concentration results in an approximately linear decrease of $V_{oc,impl}$ which indicates that the interface passivation quality suffers. Three regions can be distinguished for the $V_{oc,ext}$([B_2H_6]) dependence: (I) low doping concentration and $V_{oc,ext}$, (II) best doping concentration and $V_{oc,ext}$, and (III) very high doping concentration and reduced $V_{oc,ext}$.

It needs to be mentioned that for a-Si:H layers it is most likely not valid to assume that the relation between the [B_2H_6] concentration and the actual ionized dopant concentration in the a-Si:H layer is directly proportional. However

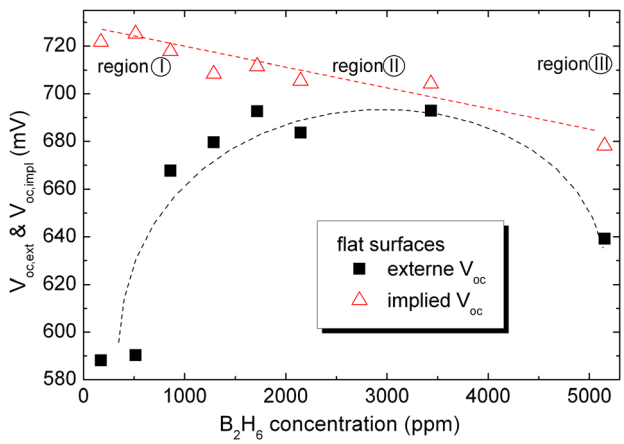

FIG. 2. (Color online) Dependence of the $V_{oc,ext}$ and $V_{oc,impl}$ measurements on the doping concentration of the a-Si:H(p) layer in an a-Si:H(i+p) layer stack. Lines are guides to the eye.

Author complimentary copy. Redistribution subject to AIP license or copyright, see http://jap.aip.org/jap/copyright.jsp

in our case a strictly monotonic increase of the ionized dopants in relation to the $[B_2H_6]$ increase can be assumed up to 3000–4000 ppm of $[B_2H_6]$. This conclusion is based on the facts: (i) The $V_{oc,impl}$ is monotonically decreasing with increasing $[B_2H_6]$ flow, and (ii) the $V_{oc,ext}$ $[B_2H_6]$ behavior (as shown in Fig. 2) and discussed in Sec. IV, can only be explained if the ionized dopant concentration increases monotonically with the $[B_2H_6]$ flow. For $[B_2H_6]$ concentrations above 4000 ppm no clear conclusion can be drawn from the data. However, we assume the active doping concentration to be reduced due to a strong increase of the defect density (see Sec. IV). Thus, based on the just described argumentation, we assume the concentration of the active doping atoms to be a quadratic function with respect to the $[B_2H_6]$ concentration/flow.

Figure 3 shows the ratio of $V_{oc,ext}$ and $V_{oc,impl}$ in dependence of the doping concentration of the a-Si:H(p) layer. This ratio will be referred as *external/internal* V_{oc}*-ratio* ζ in the following. The ζ plot in Fig. 3 shows the approach of the increasing $V_{oc,ext}$ to the dropping $V_{oc,impl}$ value. The optimum doping concentration is obtained when the ζ value approaches 1 with increasing $[B_2H_6]$ concentration, where the difference between the Fermi energies at the ITO contacts equals (approximately) to the local quasi Fermi level separation within the volume of the wafer. For a more detailed illustration of the observation presented up to now and for a better understanding of the results to be shown in the following sections, please compare the quasi Fermi level splitting illustrated in Fig. 4: solid line of the quasi Fermi level represents the optimum concentration doping case (comparable to $[B_2H_6]$ around 2100 ppm, emitter in low injection) and the broken line represents a too low doping concentration (comparable to $[B_2H_6]$ around 600 ppm, emitter in high injection). Since $V_{oc,ext}$ cannot be higher than $V_{oc,impl}$, the ζ ratio equal to one is the theoretical limit. Figure 3 can also be divided into the same three regions as depicted in Fig. 2.

For a-Si:H(p) emitters the PFF, which characterizes the series resistance free *jV*-curve measured with the *Suns-*V_{oc} set-up, is found to be dependent on the doping concentration.[8] In Ref. 8 it is suggested that the maximum value obtained for the PFF·$V_{oc,ext}$ product should be taken as a measure for the optimal doping concentration of a-Si:H(p) emitter layers.

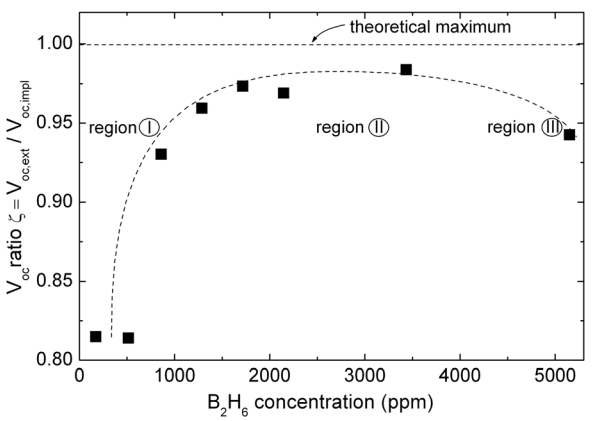

FIG. 3. *External/internal* V_{oc}-ratio ζ ($V_{oc,ext}/V_{oc,impl}$) in dependence of the doping concentration of the a-Si:H(p) layer. The V_{oc}-ratio ζ between the increase of the doping concentration and the decrease of the interface passivation is best in the region around 2000 ppm where the ratio first reaches a saturation level. Since the $V_{oc,ext}$ cannot be higher than the $V_{oc,impl}$ the ratio of 1 is the theoretical limit. The line is a guide to the eye.

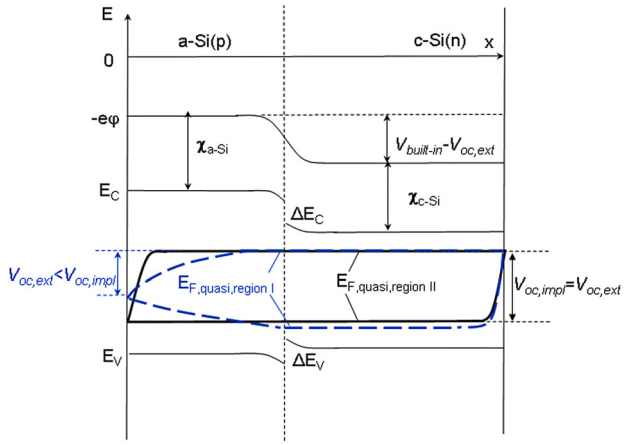

FIG. 4. (Color online) Schematic energy band diagram of an a-Si:H(p) emitter on a c-Si(n) wafer structure under illumination. Illustrated are the electron affinities $\chi_{a\text{-}Si}$, $\chi_{c\text{-}Si}$, the band off-sets ΔE_C, ΔE_V, the built-in voltage $V_{built\text{-}in}$-$V_{oc,ext}$, and the splitting of the quasi Fermi level for the doping concentration representing the regions I and II of Figs. 2 and 3.

IV. THEORETICAL ASPECTS

A. Influence of doping concentration on maximal achievable voltage

In order to gain a better theoretical understanding for the results presented in Sec. III, we present in the following our investigations of the influence of a variation of the doping concentration N_{dop} on $V_{oc,ext}$ and $V_{built\text{-}in}$ (built-in voltage) of SHJ V_{oc}-samples by analytical calculations and AFORS-HET simulations.[15] For the sake of simplicity exclusively, only the influence of the doping variation on a front side junction SHJ solar cell will be discussed. In Fig. 4 a schematic energy band diagram of an a-Si:H(p) emitter on a c-Si(n) wafer structure under illumination is shown. The electron affinities $\chi_{a\text{-}Si}$, $\chi_{c\text{-}Si}$, the band off-sets ΔE_C, ΔE_V, the built-in voltage $V_{built\text{-}in}$, $V_{oc,ext}$, and the splitting of the quasi Fermi level for the doping concentration representing regions I and II of Figs. 2 and 3 are depicted.

The $V_{built\text{-}in}$ value of any solar cell under illumination is reduced by the externally extracted voltage. This difference can be expressed analytically by the following formula (based on Ref. 16) and is illustrated in Fig. 4,

$$q\left(V_{built-in} - V_{oc,ext}\right) = \chi_{c-Si} - \chi_{a-Si} + k_B T \ln\left(\frac{p_{a-Si}}{N_{eff,VB,a-Si(p)}}\right) - k_B T \ln\left(\frac{p_{c-Si}}{N_{eff,VB,c-Si(n)}}\right), \quad (2)$$

with $\chi_{c\text{-}Si} = 3.9\,\text{eV}$ and $\chi_{a\text{-}Si} = 4.05\,\text{eV}$ representing the electron affinity of the crystalline and amorphous silicon, respectively. $N_{eff,VB,c\text{-}Si(n)} = 1.04 \times 10^{19}\,\text{cm}^{-3}$ and $N_{eff,VB,a\text{-}Si(p)} = 1 \times 10^{20}\,\text{cm}^{-3}$ represent the effective density of states of the valence band of the crystalline and amorphous silicon,

Author complimentary copy. Redistribution subject to AIP license or copyright, see http://jap.aip.org/jap/copyright.jsp

respectively. $p_{c\text{-}Si}$ depicts the minority carrier concentration at the n-type wafer back side, and $p_{a\text{-}Si}$ the majority hole carrier concentration at the a-Si:H(p) front side contact to the transparent conductive oxide. Both carrier concentrations are considered at an illumination density equal to one sun of the AM1.5 G spectrum. All parameters are taken from the AFORS-HET software.[14] For further details regarding the set of parameters applied for the simulations, please see Appendix A. Resolving Eq. (2) after $qV_{oc,ext}$ results in

$$qV_{oc,ext} = qV_{built-in} - \chi_{c-Si} + \chi_{a-Si} - k_BT \ln\left(\frac{p_{a-Si}}{p_{c-Si}}\right) + k_BT \ln\left(\frac{N_{eff,VB,a-Si(p)}}{N_{eff,VB,c-Si(n)}}\right). \quad (3)$$

The majority carrier concentration at the a-Si:H(p) to transparent conductive oxide (TCO) contact can be also expressed as $p_{a\text{-}Si} = N_{A,a\text{-}Si} + \Delta p_{a\text{-}Si}$, with $N_{A,a\text{-}Si}$ representing the doping concentration of the a-Si:H(p)-layer and $\Delta p_{a\text{-}Si}$ the hole excess carrier concentration under illumination. Furthermore, the minority carrier concentration at the c-Si(n) back contact can be expressed as $p_{c\text{-}Si} = n_i^2 \exp(\Delta E_F/k_BT)/(N_{D,c\text{-}Si} + \Delta n_{c\text{-}Si})$ with $N_{D,c\text{-}Si}$ representing the doping concentration of the c-Si(n) wafer (with a resistivity equal to 1 Ω cm) and $\Delta n_{a\text{-}Si}$ the electron excess carrier concentration under illumination. ΔE_F depicts the Fermi level splitting within the c-Si(n) wafer. All values related to the c-Si(n) wafer material are considered directly at the c-Si(n) back contact. An application of all just mentioned relations in Eq. (3) results in

$$qV_{oc,ext} = qV_{built-in} + \Delta E_F - \underbrace{k_BT \ln\left(\frac{(N_{A,a-Si} + \Delta p_{a-Si})(N_{D,c-Si} + \Delta n_{c-Si})}{n_i^2}\right)}_{\alpha} + \underbrace{k_BT \ln\left(\frac{N_{eff,VB,a-Si(p)}}{N_{eff,VB,c-Si(n)}}\right) - \chi_{c-Si} + \chi_{a-Si}}_{\beta}. \quad (4)$$

All material related values of the a-Si:H/c-Si heterojunction are summarized in the constant β. Applying the values of the electron affinities and effective densities of states as stated above, results in $\beta = 0.21$ eV. It needs to be notices that $\alpha \geq qV_{built\text{-}in} + \beta$ for all physically relevant cases.

If Eq. (2) is considered in the dark $V_{oc,ext}$ equals zero and the carrier concentration $p_{a\text{-}Si}$, $p_{c\text{-}Si}$ need to be replaced by the dark carrier concentrations $p_{a\text{-}Si,0}$ and $p_{c\text{-}Si,0}$. Furthermore $p_{a\text{-}Si,0}$ can be expressed by the doping concentration of the a-Si:H(p) layer $N_{A,a\text{-}Si}$ and $p_{c\text{-}Si,0}$ by $n_i^2/N_{D,c\text{-}Si}$. Appling all just mentioned relations in Eq.(2) and resolving for the intrinsic carrier concentration results in $n_i^2 = \exp(qV_{built\text{-}in}/k_BT + \beta)/(N_{A,a\text{-}Si}.N_{D,c\text{-}Si})$. If this relation is now inserted in Eq. (4) we end up with

$$qV_{oc,ext} = \Delta E_F - k_BT \left[\ln\left(\frac{(N_{A,a-Si} + \Delta p_{a-Si})}{N_{A,a-Si}}\right) + \ln\left(\frac{(N_{D,c-Si} + \Delta n_{c-Si})}{N_{D,c-Si}}\right)\right]. \quad (5)$$

In Eq. (5) $V_{oc,ext}$ does not depend directly on the $V_{built\text{-}in}$ any more, however the product of $N_{A,a\text{-}Si}N_{D,c\text{-}Si}$ is still included (see Eq.(4)). Based on the expression for $V_{oc,ext}$ shown in Eq. (5), it can now be concluded that a reduction of $V_{oc,ext}$ is caused if the emitter and/or the BSF are operated in high injection (i.e., $\Delta p_{a\text{-}Si} > N_{A,a\text{-}Si}$ and/or $\Delta n_{c\text{-}Si} > N_{D,c\text{-}Si}$). Thus a too low doping of the emitter or BSF layer of a SHJ solar cell results in a loss of $V_{oc,ext}$ due to losses caused by operation of the emitter and/or the BSF in high level injection and thus a gradient in the majority quasi Fermi level.

Three general rules can be listed for an optimally processed and nonlimiting doped emitter or BSF layer (region):

(i) The emitter (more precisely, the area below the metal or TCO contact area) must be in low injection for all applied illumination densities.

(ii) The BSF (more precisely, the area below the metal or TCO contact area) must be in low injection for all applied illumination densities.

(iii) The built-in voltage must be higher compared to the implied voltage. This is however only of relevance, if the emitter and the BSF region are in high injection.

B. AFORS-HET simulations

The following simulations were determined for a TCO(80 nm)/a-Si:H(p)(5 nm)/c-Si(n)(300 μm)/aluminum structure with the (free on demand) AFORS-HET software. No recombination currents at the ideal c-Si/a-Si:H interface and at the ideal, flatband, back side metal contact are taken into account. Thus in the following, we just analyze the influence of the doping variation of a front side junction SHJ solar cell for the sake of simplicity. This means we only consider an a-Si:H(p) emitter layer on top of a c-Si(n) bulk material. The application of an ideal flatband back side contact allows keeping the simulations more simple and stable, without limiting the generality of the results (see Table I for details). Since the BSF of the $V_{oc,ext}$ samples under investigation in Sec. III is assumed to be ideal, the SHJ-BSF is consequently in low injection for all measurements and does not influence $V_{oc,ext}$ and $V_{oc,impl}$. Thus the term of Eq. (5) dependent on $N_{D,c\text{-}Si}$ and

TABLE I. Parameter set for front and back side contact model applied for the AFORS-HET simulations of Secs. IV B and V B.

Front side TCO to a-Si:H(p) contact model	
Numerical model: M-S Schottky-contact (flat band)	
$SRV_{n,front}$ (cm/s)	$SRV_{p,front}$ (cm/s)
10^6	10^6
Back side c-Si(n) to Al contact model	
Numerical model: M-S Schottky-contact (flat band)	
$SRV_{n,back}$ (cm/s)	$SRV_{p,back}$ (cm/s)
10^6	10^{-5}

Author complimentary copy. Redistribution subject to AIP license or copyright, see http://jap.aip.org/jap/copyright.jsp

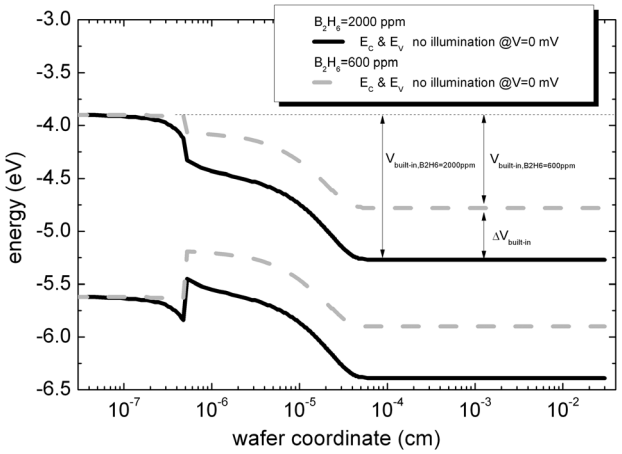

FIG. 5. Gradients of the valence- and conduction band edge for an optimum doping concentration (comparable to a doping concentration around 2000 ppm of Sect. III, solid black lines) and for a too low doping concentration (comparable to a doping concentration around 600 ppm of Sec. III, broken gray lines) without an external voltage applied and no illumination.

$\Delta n_{c\text{-}Si}$ is considered to be negligible for all $V_{oc,ext}$-samples and AFORS-Het simulations.

It is assumed that all results and conclusion made in the following for an SHJ emitter layer are transferable to an amorphous silicon back surface field.

Figure 5 shows gradients of the valence, conduction band edge, and Fermi energy for an optimum doping concentration (comparable to a doping concentration around 2000 ppm of Sec. III, solid black lines) and for a too low doping concentration (comparable to a doping concentration around 600 ppm of Sec. III, broken gray lines) without an external voltage applied and no illumination. Figure 6 shows the same devices under one sun illumination and open-circuit voltage conditions. It can be deduced from Figs. 5 and 6 that the doping concentration representing the $[B_2H_6] = 600$ ppm samples of Sec. III, results in a reduced $V_{built\text{-}in}$ and $V_{oc,ext}$, due to losses caused by an assumed high injection in the emitter (compare Figs. 5 and 6, see Eq. (5)). For the doping concentration which is assumed to represent the $[B_2H_6] = 2000$ ppm samples of Sec. III an increased

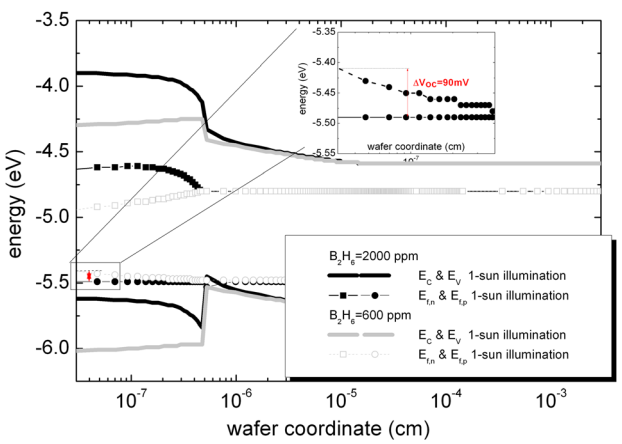

FIG. 6. (Color online) Gradients of the valence, conduction band edge, and Fermi energy for an optimum doping concentration (see in Fig. 5) and for a too low doping concentration (see in Fig. 5) under illumination and working condition around the maximum power point of the solar cell ($V = 590$ mV).

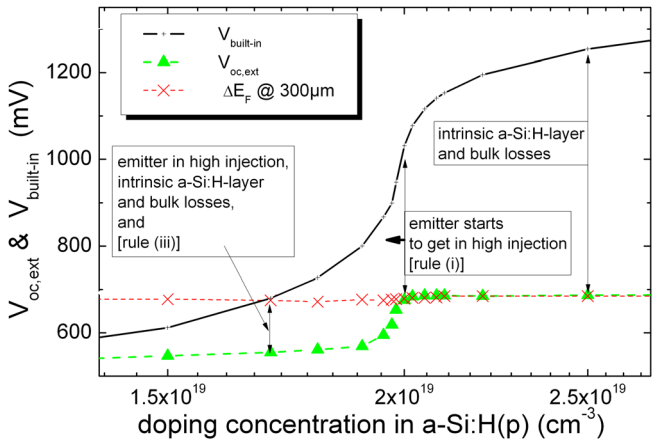

FIG. 7. (Color online) AFORS-HET simulations of the influence of the doping concentration of the a-Si:H(p)-layer (varied from $N_{dop} = 1.5 \cdot 10^{19}$ to $2.5 \cdot 10^{19}$ cm^{-3}) on $V_{oc,ext}$ and $V_{built\text{-}in}$, for a defect density present in the a-Si:H(p) of $N_{def} = 2 \cdot 10^{19}$ cm^{-3}. The Fermi level splitting within the c-Si(n) at the c-Si(n) back side (at 300 μm) as well as the difference $V_{built\text{-}in}$-$V_{oc,ext}$ are shown, too.

$V_{built\text{-}in}$ is observed (see Fig. 5) and $V_{oc,ext}$ equals $V_{oc,impl}$ very well and no high injection is assumed in the emitter layer (see Figs. 6 and 7).

In order to gain a better understanding of the influence of the doping concentration N_{dop} of the a-Si:H(p)-layer (varied from $N_{dop} = 1.5 \cdot 10^{19}$ to $2.5 \cdot 10^{19}$ cm^{-3}) on $V_{oc,ext}$ and $V_{built\text{-}in}$, AFORS-HET simulations were performed for a defect density (with a Gaussian distribution) present in the a-Si:H(p) of $N_{def} = 2 \cdot 10^{19}$ cm^{-3} (see Fig. 7 and Table II). Furthermore the Fermi level splitting within the c-Si(n) (exactly at the c-Si(n) back side, at 300 μm) is shown, too. For the calculation of the $V_{built\text{-}in}$ we need to determine the hole carrier density at the front and back interface in the dark (i.e. $V_{oc,ext} = 0$ mV, see Eq. (2)).

For $N_{dop} > 2.1 \cdot 10^{19}$ cm^{-3} (i.e. $N_{dop} > N_{def}$) the built-in voltage and $V_{oc,ext}$ saturate, and the voltage difference $V_{built\text{-}in}$-$V_{oc,ext}$ is assumed to be determined by intrinsic recombinations within the a-Si:H(p)-layer and the c-Si(n) wafer (see Fig. 7). In reference to Eq. (5) it is assumed that the emitter and the wafer are in low injection and no losses are active due to an insufficient doping of the emitter or of the bulk material (compare to region II in Fig. 2). For $N_{dop} < 2.0 \times 10^{19}$ cm^{-3} (i.e., $N_{dop} < N_{def}$) the $V_{oc,ext}$ and built-in voltage are strongly reduced, and the voltage difference $V_{built\text{-}in}$-$V_{oc,ext}$ is assumed to be limited by reduced selectivity of the *pn*-junction, and due to a high injection in the emitter region evoked by an insufficient doping (compare to region I in Fig. 2).

C. Discussion of experimental results

From Fig. 7 it can now be concluded that as long as $N_{dop} > N_{def}$, the $V_{oc,ext}$ is at a constant and high level (in our case 687 mV). Once N_{dop} comes close to N_{def}, V_{oc} starts to decrease slowly. When $N_{dop} = N_{def}$ the open-circuit voltage drops only a little to approximately 99% of its maximum value. If we assume that for the a-Si:H(p) layers under investigation (Sec. III, Figs. 2 and 3) N_{dop} is equal to N_{def} in the $[B_2H_6]$ doping concentration range between 1500 and 2000 ppm, we can conclude a good agreement with the data

Author complimentary copy. Redistribution subject to AIP license or copyright, see http://jap.aip.org/jap/copyright.jsp

TABLE II. Parameter set for the midgap defect density, Urbach-tail defects, a-Si:H(p)-layer, and c-Si(n) wafer applied for the AFORS-HET simulations of Secs. IV B and V B.

a-Si:H(p) parameter		Midgap defects (Gauss)		Urbach-tail defects	
e_k (-)	11.9	acceptor defects		valence-tail	
$c_{a\text{-}Si}$ (eV)	3.9	$N_{tr,total}$ (cm^{-3})	$(2\text{-}3)\cdot10^{19}$	$N_{tr,total}$ (cm^{-3})	$1.38\cdot10^{20}$
$E_g = E_{g,opt}$ (eV)	1.72	c_n (cm^{-3})	$1.3\cdot10^{-14}$	c_n (cm^{-3})	$7\cdot10^{-16}$
$N_c = N_v$ (cm^{-3})	10^{20}	c_p (cm^{-3})	$3\cdot10^{-14}$	c_p (cm^{-3})	$7\cdot10^{-16}$
μ_e (cm^2/Vs)	5	$E_{gau\beta}$ (eV)	1.2	$E_{VB,tail}$ (meV)	68.8
μ_h (cm^2/Vs)	1	donator defects		conduct-tail	
N_a (cm^{-3})	$(1\text{-}5)\cdot10^{19}$	$N_{tr,total}$ (cm^{-3})	$(2\text{-}3)\cdot10^{19}$	$N_{tr,total}$ (cm^{-3})	$7\cdot10^{19}$
N_d (cm^{-3})	0	c_n (cm^{-3})	$3\cdot10^{-14}$	c_n (cm^{-3})	$7\cdot10^{-16}$
$v_e = v_h$ (cm/s)	10^7	c_p (cm^{-3})	$3\cdot10^{-15}$	c_p (cm^{-3})	$7\cdot10^{-16}$
ρ (g cm^{-3})	2.328	$E_{gau\beta}$ (eV)	1.1	$E_{CV,tail}$ (eV)	35
d (nm)	5	$s_{acc} = s_{don}$ (eV)	0.22		

shown in Fig. 2 and 3 and the simulations shown in Fig. 7. In case the just mentioned conclusion is valid, this may open a new potential to determine the total active defect density of an ultra thin, active a-Si:H(p) layer included in a working device with a comparison of $V_{oc}([B_2H_6])$ values of differently deposited a-Si:H(p) layers. In the case that $N_{dop} < N_{def}$ a significant drop of $V_{built\text{-}in}$ and$V_{oc,ext}$ is observed (see Fig. 7). Since N_{def} represents the peak position of a Gaussian distribution of mid gap defects $N_{dop} < N_{def}$ does not mean that there are no active doping atoms left. For $N_{dop} < N_{def}$ there are still active doping atoms, however, they are reduced drastically with the decrease of N_{dop}.

A more precise description of the defect states present in the a-Si:H(p) would take into account that N_{def} (as stated up to now) represents only the peak position of a Gaussian distribution of midgap defects and thus does not consider all other defect state above and below the peak defect state concentration. The same argument can be applied for a more realistic description of the actually present doping concentration. Hence a Gaussian distribution of the doping states should be also taken into account for the a-Si:H(p or n) layers. Since the AFORS-HET software offers only the opportunity to consider the Gaussian distribution of the defect states, all above state and all following discussions are related to the peak concentrations of N_{def} and N_{dot}. It is assumed that this simplification is not limiting the general conclusions drawn in the following.

All investigations shown above lead us to the conclusion that for silicon heterojunction solar cells the apparent doping concentration $N_{app} \cong N_{dop} - N_{def}$ is the main parameter to achieve the maximum voltage. Thus in case of the results shown in Fig. 2 we assume $N_{dop} < N_{def}$ (small N_{app}) for the increasing part of the $V_{oc}([B_2H_6])$ (region I), and $N_{dop} > N_{def}$ (high N_{app}) for the saturating part (region II). Furthermore, we suggest that the decreasing part of the $V_{oc}([B_2H_6])$ correlation (region III) can be understood as follows: It is known that the defect density increases with an rising doping concentration.[4] Thus we assume N_{app} to become very small again in region III. Hence for excessively high doping concentrations N_{def} is assumed to increase faster with a rising doping concentration than N_{dot} itself. Furthermore, the processed V_{ext}-samples are also influenced by the increased interface recombination which additionally reduces the considered voltages. In real SHJ solar cells N_{def} represents a total defect density combining both the defect states in the a-Si:H layers and at the a-Si:H/c-Si interface.

V. ILLUMINATION DEPENDENCE

A. Measurements of the illumination dependence of $V_{oc,ext}$ and $V_{oc,impl}$

In order to gain a deeper insight into the physics, a comparison of $V_{oc,ext}$ to $V_{oc,impl}$ illumination-dependent measurements have been performed. Figure 8 shows $V_{oc,ext}$ over $V_{oc,impl}$ for varying illumination density. The angle dissector line represents the *external/internal* V_{oc}*-ratio* $\zeta = 1$ and thus a good balance between the best interface passivation and a sufficient doping of the emitter. This statement is only true for the lowest doping concentration that guarantees $\zeta = 1$. A higher concentration can still result in $\zeta = 1$. However, the implied voltage would be reduced by an increased defect

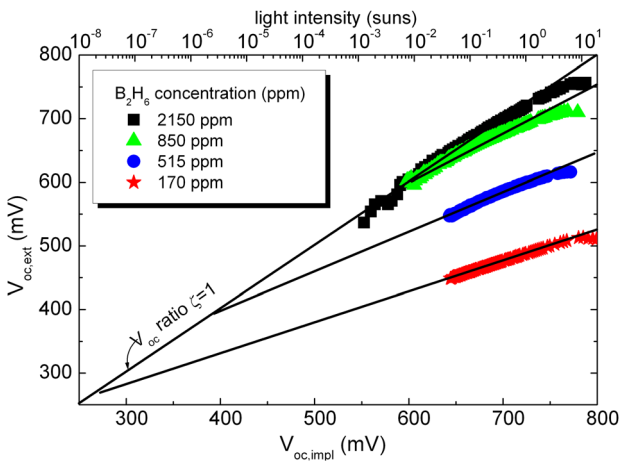

FIG. 8. (Color online) $V_{oc,ext}$ and the implied voltage are plotted against each other for different illumination intensities and doping concentrations. The angle dissector line represents the ratio of 1 between the $V_{oc,ext}$ and $V_{oc,impl}$. The light intensity values shown at the upper x-axis are only accurate for the 2150 ppm sample. For all other samples, the light intensity values represent only estimates.

Author complimentary copy. Redistribution subject to AIP license or copyright, see http://jap.aip.org/jap/copyright.jsp

density in the emitter layer and at the interface. The sample with the highest doping concentration of 2150 ppm shown in Fig. 8 is the only one that exhibits the ratio ζ close to the illumination densities around one sun (compare Sec. III). For this sample all measurement points are lined up along the angle dissector line for illumination densities smaller than one sun. A reduction of the doping concentration down to 170 ppm results in a decrease of the ratio and a lower slope of the $V_{oc,ext}$ over $V_{oc,impl}$ plot (see Fig. 8). A line fit to each measurement point set brings us to the conclusion that with a lower doping concentration the cross section point between the fit-line and the angle dissector line is shifted to lower illumination densities. With a reduction of the injection level for the lower doped emitter the level of high injection is reduced and ζ closer to unity. At the illumination density given by the cross point of the angle dissector line and the line fit of the measurements points we observe an *external/internal* V_{oc}*-ratio* $\zeta = 1$ for the present doping concentration of the investigated sample. Hence reducing the doping concentration below the optimum results in a decline of the cross-section point. This section is considered as a reference system for the following simulation.

B. AFORS-HET simulation of the illumination dependence

In order to confirm the measurements and drawn conclusions presented in Sec. V A, AFORS-HET simulations have been performed for various illumination densities (see Fig. 9). The determined $V_{oc,ext}$ values were directly extracted from the AFORS-HET software. The minority/majority carrier densities, which are present in the c-Si(n) wafer have been used to calculate the implied voltage by the application of Eq. (1) (see Fig. 9). The total defect density N_{def} in the a-Si:H(p) layer and its doping concentration N_{dot} have been varied.

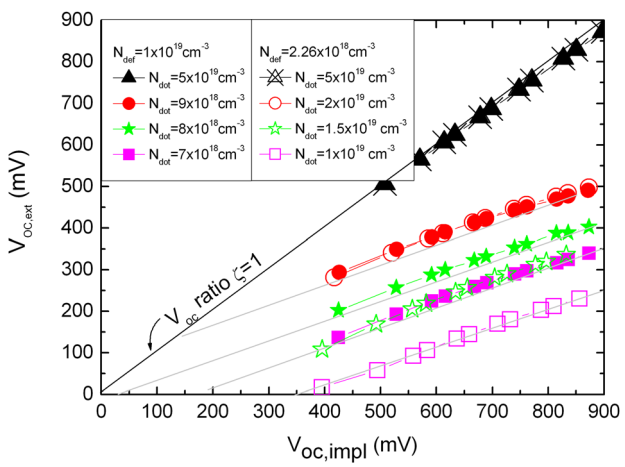

FIG. 9. (Color online) $V_{oc,ext}$ and implied voltage determined using AFORS-HET simulation software for different illumination densities. The total mid gap defect density N_{def} in the a-Si:H(p) layer and the doping concentration N_{dot} have been varied. An n-type crystalline wafer with a ideal Al-rear side metallization ($S_p = 1 \cdot 10^{-3}$ cm/s and $S_p = 1 \cdot 10^6$ cm/s), an 5 nm a-Si:H(p) layer, and 80 nm of TCO on top was simulated. No interface defect density has been taken into account.

Very similar results can be observed for the simulation and the experimental measurements shown in Sec. V A (compare Figs. 8 and 9). With a reduction of the doping concentration the slope of the $V_{oc,ext}$ versus $V_{oc,impl}$ plot decreases and the cross-section point between the angle dissector line and the measurement point line-fit declines (see Figs. 8 and 9). Furthermore, it can be concluded that an increase of the total defect density in the a-Si:H(p) layer reduces the ratio of $V_{oc,ext}$ to $V_{oc,impl}$ and the angle dissector line cross-section point. Thus for a-Si:H(p) layers with a higher quality (less defects) a lower doping concentration is needed to reach the same $V_{oc,ext}$ value.

Based on the investigations presented in Secs. V A and V B the rough optimization approach is suggested, which can be followed by analyzing the following questions: (i) Are the measurement points lined up on the angle dissector line? If so, the doping concentration is good, however, it may even be too high. (ii) Are the measurement points lined up below the angle dissector line? In that case, bigger problems are present in the construction of the solar cell (e.g., a too low doping concentration or a to high defect density N_{def}). A parallel shift of the measurement point down to lower $V_{oc,ext}$ values can be interpreted as an increase in the defect density of the a-Si:H layer and thus a lowering of the present built-in voltage and/or the emitter (or BSF) layer is assumed to be in high level injection.

VI. CONCLUSION

In this publication we presented that a comparison of the open circuit voltage V_{oc} values: (i) external voltage $V_{oc,ext}$ (determined by *Suns-*V_{oc} measurements) to (ii) implied voltage $V_{oc,impl}$ (determined by transient photoconductance decay lifetime measurements) can lead to a quick and easy analysis and characterization of SHJ solar cells, especially in regard to finding the optimum doping concentration of the emitter or BSF layer. The $V_{oc,impl}$ represents the interface passivation and bulk quality. The $V_{oc,ext}$ value additionally gives a measure of the active doping concentration. Increasing the concentration of dopants during the deposition of, e.g. an a-Si:H(p) layer reduces the interface passivation quality ($V_{oc,impl}$) and increases the external voltage $V_{oc,ext}$ value. The best *external/internal* V_{oc}*-ratio* ζ is realized when the ratio of $V_{oc,ext}$ to $V_{oc,impl}$ first comes to a saturation point near one with an increasing doping concentration. Excessive doping concentrations impairs both $V_{oc,ext}$ and $V_{oc,impl}$.

AFORS-HET simulations and theoretical considerations resulted in the conclusions that the externally extractable voltage $V_{oc,ext}$ is mainly influenced by the operation conditions (high or low injection) of the doped layers and by the built-in voltage. Both influencing factors just mentioned are mainly determined by the apparent doping concentration (doping minus defect concentration).

Furthermore, $V_{oc,ext}$ and $V_{oc,impl}$ values have been measured and simulated (using AFORS-HET) in dependence of the illumination density, doping concentration, and the total defect density of a-Si:H(p) layers in regard to their influence on the passivation quality and built-in voltage. These

Author complimentary copy. Redistribution subject to AIP license or copyright, see http://jap.aip.org/jap/copyright.jsp

investigations led us to a deepened physical understanding of the SHJ emitter system.

ACKNOWLEDGMENTS

The authors would like to thank S. Seitz, T. Leimenstoll, A. Stifel, T. Boritzka, I. Druschke, F. Schaetzle, A. Filipovic, and E. Schäffer for process technology, simulation support, and measurements. The work has been supported by the German Federal Ministry for the Environment, Nature Conservation and Nuclear Safety under Contract No. 0329849 A "Th-ETA."

APPENDIX A: PARAMETER SET FOR ALL AFORS-HET SIMULATIONS

Table II shows the parameter set applied for all AFORS-HET simulations of the investigations presented in Secs. IV B and V B. All abbreviations shown in Table II have exactly the same notation as used in the AFORS-HET software and are well described therein.

APPENDIX B: PARAMETER SET OF THE IDEAL CONTACT MODEL

Table I shows the parameter set of the applied ideal contact model at the front and back side of all AFORS-HET simulations conducted for the investigation presenter in the Secs. IV B and V B. All abbreviations show in Table II have exactly the same notation as used in the AFORS-HET software and are described therein.

[1]T. Sawada, N. Terada, S. Tsuge, T. Baba, T. Takahama, K. Wakisaka, S. Tsuda, and S. Nakano, paper presented at the Proceedings of the 1st World Conference on Photovoltaic Energy Conversion, Waikoloa, HI, Dec. 5-9, 1994.
[2]S. Taira, Y. Yoshimine, T. Baba, M. Taguchi, and H. Kanno, paper presented at the Proceedings of the 22nd European Photovoltaic Solar Energy Conference, Milan, Italy, 2007.
[3]L. Korte and M. Schmidt, J. Non-Cryst. Solids **354**, 21382143 (2008).
[4]L. Korte, E. Conrad, H. Angermann, R. Stangl, and M. Schmidt, Sol. Energy Mater. Sol. Cells **93**, 905 (2009).
[5]A. Laades, Ph.D. dissertation, Technische Universität Berlin, 2005.
[6]D. M. Cervantes, Ph.D. dissertation, Universitat Politécnica de Catalunya, 2008.
[7]R. A. Sinton and A. Cuevas, Appl. Phys. Lett. **69**, 2510 (1996).
[8]D. Pysch, C. Meinhardt, M. Hermle, and S. W. Glunz, paper presented at the Proceedings of the 25th European Photovoltaic Solar Energy Conference and Exhibition, Valencia, Spain, 2010.
[9]R. A. Sinton, A. Cuevas, and M. Stuckings, paper presented at the Proceedings of the 25th IEEE Photovoltaic Specialists Conference, Washington, D.C., USA, 1996.
[10]R. A. Sinton and A. Cuevas, paper presented at the Proceedings of the 16th European Photovoltaic Solar Energy Conference, Glasgow, United Kingdom, 2000.
[11]A. Richter, J. Benick, and S. W. Glunz, paper presented at the Proceedings of the 23rd European Photovoltaic Solar Energy Conference, Valencia, Spain, May 9, 2008.
[12]J.- P. Becker, D. Pysch, A. Leimenstoll, M. Hermle, and S. W. Glunz, paper presented at the Proceedings of the 24th European Photovoltaic Solar Energy Conference, Hamburg, Germany, September 25, 2009; H. Angermann, J. Rappich, and C. Klimm, Cent. Eur. J. Phys. **7**, 363 (2009).
[13]D. Pysch, M. Bivour, K. Zimmermann, C. Schetter, M. Hermle, and S. W. Glunz, paper presented at the Proceedings of the 24th European Photovoltaic Solar Energy Conference, Hamburg, Germany, September 25, 2009.
[14]M. Wolf and H. Rauschenbach, Advanced Energy Conversion **3**, 455 (1963).
[15]A. Froitzheim, R. Stangl, L. Elstner, M. Kriegel, and W. Fuhs, paper presented at the Proceedings of the 29th IEEE Photovoltaics Specialists Conference, New Orleans, Louisiana, USA, 2002.
[16]P. Würfel, *Physics of Solar Cells - From Principles to New Concepts*. (Wiley-VCH Verlag GmbH, Weinheim, 2005).

Author complimentary copy. Redistribution subject to AIP license or copyright, see http://jap.aip.org/jap/copyright.jsp